Available online at www.sciencedirect.com

ScienceDirect

Proceedings of the Combustion Institute 35 (2015) 2563–2571

Proceedings of the Combustion Institute

www.elsevier.com/locate/proci

Numerical simulation of under-ventilated liquid-fueled compartment fires with flame extinction and thermally-driven fuel evaporation

S. Vilfayeau [a], N. Ren [b], Y. Wang [b], A. Trouvé [a,*]

[a] Department of Fire Protection Engineering, University of Maryland, College Park, MD 20742, USA
[b] FM Global, Research Division, Norwood, MA 02062, USA

Available online 21 June 2014

Abstract

Compartment fires exhibit unique features associated with smoke accumulation and restricted air ventilation. The objective of the present study is to evaluate the ability of CFD-based fire models to simulate these features and in particular the effects of flame extinction that results from under-ventilated fire conditions. The study is performed using FireFOAM; FireFOAM is an advanced fire modeling software developed by FM Global and is based on a general-purpose open-source software called OpenFOAM. A new flame extinction model based on the concept of a critical value of the flame Damköhler number is incorporated into FireFOAM. The performance of the extinction model is evaluated via comparisons with a previously developed experimental database corresponding to a reduced-scale, heptane-fueled, compartment fire configuration. The numerical simulations also include a description of fuel evaporation driven by the computed gas-to-liquid heat feedback. Comparisons between experimental data and numerical results provide a suitable test bed to evaluate the ability of CFD-based fire models to describe the transition from over- to under-ventilated fire conditions, as well as the transition from extinction-free conditions to conditions in which the flame experiences partial or total quenching.

Keywords: Under-ventilated fires; Diffusion flame extinction; Combustion efficiency; Fuel evaporation; Large eddy simulation.

1. Introduction

The simulation of fire phenomena using classical Computational Fluid Dynamics (CFD) methods has made remarkable progress in the past 20 years. Two of the main challenges found in a CFD treatment of compartment fires are the possible transition to under-ventilated combustion and the sensitivity of the production rate of flammable vapors (*i.e.*, the fuel) to the fire room thermal environment [1].

The transition to under-ventilated combustion is typically observed as a consequence of a rapid increase in fire size called flashover. After flashover has occurred, the conditions inside the fire compartment switch from a fuel-limited to an

* Corresponding author. Address: University of Maryland, 3104D J.M Patterson Bldg., College Park, MD 20742-3031, USA. Fax: +1 301 405 9383.
E-mail address: atrouve@umd.edu (A. Trouvé).

http://dx.doi.org/10.1016/j.proci.2014.05.072
1540-7489/

oxygen-limited combustion regime. This combustion regime is characterized by an increased probability of flame extinction and increased emissions of products of incomplete combustion. It is also associated with a dramatic change in flame structure in which the flame is observed to migrate from the fuel sources towards the compartment vents, *i.e.*, towards the oxygen supply streams.

The occurrence of flame extinction is a challenge for combustion modeling in general, and for fire modeling in particular. Diffusion flames may be extinguished by a number of different mechanisms, *i.e.*, by aerodynamic, thermal or dilution quenching [2–9]. Laminar flame theory suggests that all these different mechanisms may be explained by a single flame extinction criterion known as a Damköhler number criterion [2–4]: the Damköhler number Da is defined as the ratio of a characteristic fuel–air mixing time divided by a characteristic chemical time, $Da = (\tau_{mixing}/\tau_{chemical})$, and extinction is predicted to occur for values of Da that are critically low. Theoretical analysis shows that the characteristic mixing time τ_{mixing} scales like the inverse of flame stretch, noted χ_{st}, with χ_{st} defined as the stoichiometric value of the scalar dissipation rate; theoretical analysis also shows that the characteristic chemical time $\tau_{chemical}$ scales like $\exp(T_a/T_{st})$, where T_{st} is the flame temperature and T_a an activation temperature (assuming Arrhenius-like combustion chemistry, T_a gives a measure of the sensitivity of the combustion chemistry to changes in temperature). Thus, we find that the Damköhler number is a function of flame stretch and flame temperature, $Da \sim (1/\chi_{st})/\exp(T_a/T_{st})$. Figure 1 presents a typical flammability map obtained for heptane-air non-premixed combustion; this map has been constructed using large activation energy asymptotic theory [9].

The discussion on the flame Damköhler number serves to illustrate some of the current challenges found in combustion modeling since it shows that flame extinction is controlled by flame-based quantities like stretch and temperature that are typically unresolved in a CFD simulation. The occurrence of flame extinction may also be followed by re-ignition and the modeling of under-ventilated fires requires both an extinction model and a re-ignition model.

Another challenge found in fire modeling is the description of the fuel source(s). Assuming a liquid or solid fuel source, a fire may be described as a closed-loop heat feedback system in which the gas-to-fuel-source heat flux (also called the thermal feedback) controls the production rate of flammable vapors (also called the fuel mass loss rate or MLR); MLR and the resulting combustion process control in turn the intensity of the thermal feedback. The simulation of (solid fuel) pyrolysis or (liquid fuel) evaporation processes requires an accurate representation of the thermal feedback.

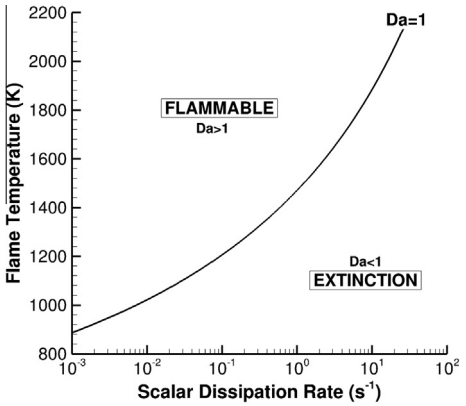

Fig. 1. Flammability map for heptane-air laminar diffusion flames using flame stretch, χ_{st}, and flame temperature, T_{st}, as coordinates. The solid line corresponds to the extinction limit, Da = 1 [9].

The exact level of grid resolution required for accurate representations of heat fluxes is unknown but recent evidence suggests that sub-centimeter grid sizes may be required [10].

The objective of the present study is to evaluate the ability of current CFD-based fire modeling capabilities to treat flame extinction and thermally-driven MLR. The developments and tests are made in the context of a CFD solver called FireFOAM [11]. The present study proposes a new flame extinction model based on the concept of a critical value of the flame Damköhler number; the model is implemented into FireFOAM and evaluated with a thermally-driven MLR model. This study is a continuation of earlier work [12,13]. The earlier work was performed using a different solver (called FDS) and using a simple flame extinction model based on the concept of a critical value of the flame temperature; note also that the emphasis in Refs. [12,13] was primarily on simulations performed with a prescribed MLR approach.

The experimental (numerical) configuration is described in Section 2.1 (Sections 2.2 and 2.3). The new diffusion flame extinction model is presented in Section 2.4. Model performance is evaluated in Section 3.

2. Modeling approach

2.1. Experimental configuration

The experimental configuration is a reduced-scale compartment previously studied at the University of Maryland [14,15]. The compartment is cubic-shaped and has a 40 cm size. The walls are made of type-M Kaowool® board. The compartment is vented by two identical slots located near the top and bottom of one of the vertical walls.

Combustion inside the compartment is fueled by a round-shaped heptane pool centrally-located on the compartment floor. The global equivalence ratio inside the compartment is modified using different vent dimensions (*i.e.*, different values of the width W_v and height H_v of the vents) and different fuel pan sizes (*i.e.*, different diameters D). Details about the instrumentation may be found in Refs. [14,15].

A wide variety of flame behaviors is observed in the experimental database [14,15]. These flame behaviors belong to one of the following four categories: (R1) steady well-ventilated fires in which the flame is stabilized above the burner; (R2) steady under-ventilated fires in which the flame is stabilized near the vents; (R3) unsteady under-ventilated fires featuring large periodic oscillations and intermittent flame quenching; (R4) unsteady under-ventilated fires leading to complete flame extinction. The main parameter that controls transition from one flame regime to another has previously been identified as the fire room global equivalence ratio (GER). In short, regime R1 corresponds to small values of GER, regime R4 to large values, regime R3 to values close to 1 and regime R2 to values slightly above 1. Table 1 presents the parameters of the 3 cases considered in the present study (we call these cases by the name of the regimes they are selected to represent).

2.2. Numerical solver

FireFOAM [11,16] is based on OpenFOAM, a free, open-source, general-purpose, CFD software [17]. OpenFOAM is an object-oriented, C++-based, second-order accurate, finite volume solver with implicit time integration; the solver features advanced meshing capabilities (structured/unstructured polyhedral mesh) and a massively parallel computing capability using MPI protocols.

FireFOAM is a large eddy simulation (LES) fire dynamics solver that uses a Favre-filtered compressible flow formulation and provides a choice between several modeling options for the treatment of turbulence, combustion and thermal radiation. In the present study, subgrid-scale (SGS) turbulence is described using the k-equation eddy viscosity model; this model is based on solving a transport equation for the SGS turbulent kinetic energy k_{sgs} [16]. Note that in this model, the SGS turbulent mixing time scale is $\tau_t = (1/C_e) \times (\Delta/k_{sgs}^{1/2})$, where Δ is the local LES filter size (defined as the cubic root of the volume of the computational cell) and $C_e = 1.048$ [18].

In FireFOAM, combustion is described using a global single-step combustion equation combined with the Eddy Dissipation Concept (EDC) model [19]. In EDC, the fuel mass reaction rate is expressed as:

$$\overline{\dot{\omega}'''_{EDC}} = C_{EDC}\frac{\bar{\rho}}{\tau_t}\min\left(\tilde{Y}_{C_7H_{16}}, \frac{\tilde{Y}_{O_2}}{r_s}\right), \quad (1)$$

where $\bar{\rho}$ is the (LES-filtered) mass density, $\tilde{Y}_{C_7H_{16}}$ and $\tilde{Y}_{O_2}$ the (LES-filtered) fuel and oxygen mass fractions, r_s the stoichiometric oxygen-to-fuel mass ratio, and $C_{EDC} = 4$.

In FireFOAM, the radiative transfer equation (RTE) is solved using the discrete ordinate method [16]. In the present study, the description of thermal radiation is simplified by assuming a gray and non-absorbing, optically-thin medium. The flame emission is described using the concept of a radiant fraction χ_{rad} [16]; we use $\chi_{rad} = 35\%$ [20]. The assumption of a non-absorbing medium is deemed acceptable in the present small-scale configuration. This assumption should be viewed as an intermediate step that conveniently avoids the difficulties associated with modeling soot formation.

2.3. Numerical configuration

The computational domain includes the fire compartment and an adjacent air block (Fig. 2). The role of the air block is to avoid treating the vents as numerical boundary conditions and to bring more accuracy to the simulated vent flows. The fire compartment (adjacent air block) is $40 \times 40 \times 40\ cm^3$ ($40 \times 40 \times 60\ cm^3$). The computational mesh inside the fire compartment is unstructured and uses 145,680 triangular prisms; the mesh resolution Δ_m is approximately 1 cm. The computational mesh in the air block is structured and uses a stretched rectangular grid with 55,000 cells.

Note that the present choices correspond to a trade-off between expected accuracy and computational cost and do not follow all recommended guidelines for grid design. The configuration shown in Fig. 2 features three types of relevant

Table 1
Ventilation and fuel source parameters in cases R1, R2 and R4. The global equivalence ratio in column 4 is estimated using average values of the measured fuel evaporation rate and vent flow rate of incoming fresh air.

Case	Vent height × Width (cm)	Fuel Pan Diameter (cm)	GER
R1	3 × 40	9.5	0.2
R2	1 × 40	19	2.6
R4	1 × 2	9.5	12.0

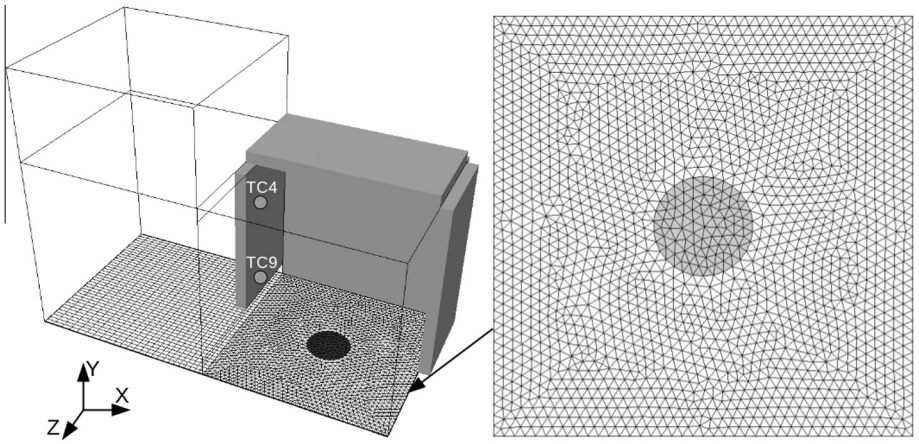

Fig. 2. Numerical configuration showing the fire compartment and the adjacent air block. The compartment features a floor-level circular fuel pan and two vents located at the top and bottom of the west wall. The figure shows the footprint of the computational mesh (on the plane $z = 0$): the mesh is unstructured in the fire compartment. The figure also shows the location of the thermocouples (TC4/TC9) used in subsequent figures.

length scales: the flame scales (the width and height of the flame, which are related to the fuel pan diameter), the vent flow scales (the width and height of the vents) and the wall flow scales (the thickness of the thermal boundary layers). Recommended guidelines in fire modeling suggest using a mesh with characteristic ratios (D/Δ_m), (H_v/Δ_m) and (W_v/Δ_m) greater than 10. With our choices, the resolution of the flame region is marginal, $(D/\Delta_m) \approx 9.5$ in cases R1 and R4, while that of the vent flows is generally poor, $(H_v/\Delta_m) = 1$ in cases R2 and R4 (Table 1). Note that, while the vent flows are clearly under-resolved, tests have shown that the simulated vent mass flow rates are in good agreement with measurements from Refs. [14,15]; one possible explanation is that the magnitude of the vent flow rates is primarily determined by pressure differences between the compartment and the outside and that correct predictions of pressure differences may not require resolving the details of the vent flow. Finally, while the exact thickness of the wall boundary layers is unknown, numerical tests have shown that the convective heat transfer is responsible for less than 25% of the thermal feedback to the liquid fuel and also for less than 25% of the heat flux to the solid walls; the possible lack of resolution in the boundary layers has therefore limited impact on the present simulations. Based on this evidence, the current grid choices are deemed acceptable.

We now turn to a discussion of the model for liquid fuel evaporation. The heptane pool surface boundary conditions correspond to a constant position (liquid regression is neglected), a prescribed temperature (we use 98 °C equal to the boiling point of heptane) and a mass evaporation rate, noted $\dot{m}''_f$ (in units of kg/s/m^2), that is treated as proportional to the net total gas-to-liquid heat flux, noted $\dot{q}''_s$. We write: $\dot{m}''_f = (\dot{q}''_s/\Delta H_v)$ where ΔH_v is an effective heat of vaporization. Note that, while the thermodynamic value of ΔH_v for heptane is equal to 0.45 MJ/kg, the apparent values of ΔH_v in Refs. [14,15] (calculated as the ratio of $\dot{q}''_s$ divided by $\dot{m}''_f$ with $\dot{q}''_s$ measured with a heat flux gauge and $\dot{m}''_f$ measured with a load cell) are much larger: $\Delta H_v = 2$ MJ/kg for cases R1 and R4, and $\Delta H_v = 1$ MJ/kg for case R2 (featuring a larger fuel pan). These high values may be interpreted as effective heats of vaporization that account for unresolved physics, *e.g.*, heat losses to the fuel container walls, *etc*. These results suggest that an accurate representation of evaporation processes may require using an advanced heptane pool model with a detailed representation of the in-liquid heat transfer. In the present study, we choose instead to use the experimentally-determined effective heats of vaporization. In order to avoid possible uncontrolled oscillations and to represent thermal inertia effects in the heptane pool, the gas-to-liquid heat flux is both spatially-averaged (across the pool surface) and time-averaged (over a period of 4 s); we write: $\dot{m}_f'' = (\int\int \overline{\dot{q}''_s} dA_f/\Delta H_v)A_f$, where A_f is the pool surface area, and where $\overline{\dot{q}''_s}(t) = \int_{t-4s}^{t} \dot{q}''_s(t')dt'$. Finally, burn-out is described using an *ad hoc* model that increases ΔH_v when the residual fuel mass is close to 0.

An important element in modeling compartment fires is the wall convective heat transfer model. Our model is based on a classical gradient diffusion modeling approach with a turbulent diffusivity; no law of the wall is used; the wall temperatures are calculated using a standard conjugate heat transfer approach and use a one-dimensional solver to treat heat conduction

normal to the solid walls. As mentioned above, convective heat transfer is believed to have limited impact on the present simulations.

2.4. Flame extinction model

We present in this section the new flame extinction model implemented into FireFOAM. The combustion model in FireFOAM uses a classical global combustion equation: $C_7H_{16} + 11O_2 \rightarrow 7CO_2 + 8H_2O$ (GR1). Global reaction (GR1) corresponds to a normal combustion step for heptane fuel. When considering extinction, reaction (GR1) is enhanced by two additional steps: $C_7H_{16} \rightarrow (C_7H_{16})^*$ (GR2); $(C_7H_{16})^* + 11O_2 \rightarrow 7CO_2 + 8H_2O$ (GR3), where global reaction (GR2) describes the flame extinction phenomenon, treated as a transformation of fresh fuel C_7H_{16} into non-burning fuel $(C_7H_{16})^*$, and global reaction (GR3) describes the re-ignition phenomenon, treated as a normal combustion step for $(C_7H_{16})^*$. The list of transported species in our model includes C_7H_{16}, $(C_7H_{16})^*$, O_2, CO_2 and H_2O.

The closure expressions for the chemical reaction rates are based on the EDC model [18]: $\overline{\dot{\omega}'''_{GR1}} = (1 - FEF) \times \overline{\dot{\omega}'''_{EDC}}$, $\overline{\dot{\omega}'''_{GR2}} = FEF \times \overline{\dot{\omega}'''_{EDC}}$ and $\overline{\dot{\omega}'''_{GR3}} = FIF \times \overline{(\dot{\omega}'''_{EDC})^*}$, where $\overline{\dot{\omega}'''_{EDC}}$ and $\overline{(\dot{\omega}'''_{EDC})^*}$ are the EDC-based fuel and non-burning fuel consumption rates (see Eq. (1)). In the expressions above, FEF and FIF respectively designate a flame extinction factor and a flame re-ignition factor; these factors take values between 0 and 1 and give a measure of the local probabilities of extinction and re-ignition phenomena: $FEF = 0$ ($FIF = 0$) for cases without flame extinction (re-ignition); $FEF = 1$ ($FIF = 1$) for cases with complete extinction (re-ignition). The corresponding expression for the heat release rate per unit volume is: $\overline{\dot{\omega}'''_{h_s}} = (\overline{\dot{\omega}'''_{GR1}} + \overline{\dot{\omega}'''_{GR3}}) \times \Delta H_F$, where ΔH_F is the heat of combustion (per unit mass of fuel); we use $\Delta H_F = 42$ MJ/kg.

Flame extinction is treated via a critical Damköhler number criterion: $FEF = 0$ if $Da \geqslant Da_c$ and $FEF = 1$ if $Da < Da_c$, where Da is the flame Damköhler number and Da_c its critical value at extinction. We use $Da_c = 1$ [8,9] and write:

$$Da = C \times \frac{exp(-T_a/T_{st})}{\chi_{st}} \tag{2}$$

where C is a model coefficient. C and T_a are fuel-dependent properties that are calibrated by comparison with experimental data on extinction limits of heptane-air laminar diffusion flames [21]; we use $C = 36{,}140\ s^{-1}$ and $T_a = 15{,}430$ K. The flame-based quantities T_{st} and χ_{st} used in Eq. (2) are obtained via subgrid-scale models and are discussed next.

The SGS flame temperature T_{st} in Eq. (2) is estimated from a modified mixture-fraction-based Burke–Schumann model:

$$T_{st} = (1 + H_{st})T^{ad}_{st} - H_{st}T^{m}_{st} \tag{3}$$

where T^m_{st} is a pure mixing temperature (the temperature that would be obtained as a result of fuel–air mixing and without combustion; we use $T^m_{st} = 298$ K), T^{ad}_{st} the adiabatic flame temperature (we use $T^{ad}_{st} = 2300$ K), and H_{st} an excess enthalpy variable introduced to provide a measure of the magnitude of non-adiabatic effects ($H_{st} = 0$ under adiabatic burning conditions; $H_{st} = -1$ under non-burning conditions). H_{st} is obtained from a comparison between the (LES-filtered) total enthalpy $\tilde{h}$ and the Burke–Schumann expression for the expected adiabatic value of total enthalpy, noted $h^{ad}(\tilde{Z})$, with $\tilde{Z}$ the (LES-filtered) mixture fraction: $H_{st} = (\tilde{h} - h^{ad}(\tilde{Z}))/min[(\tilde{Z}/Z_{st}), (1 - \tilde{Z})/(1 - Z_{st})]/(Z_{st}\Delta H_F)$, where Z_{st} is the stoichiometric value of mixture fraction; $\tilde{Z} = ((\tilde{Y}_{O_2,\infty}/r_s) - (\tilde{Y}_{O_2}/r_s) + (\tilde{Y}_{CO_2}/\eta_{CO_2}))/(\tilde{Y}_{O_2,\infty}/r_s)$, where $\tilde{Y}_{O_2,\infty}$ is the oxygen mole fraction in ambient air and η_{CO_2} is the CO_2 yield.

The SGS flame stretch χ_{st} in Eq. (2) is estimated from a classical laminar flamelet expression:

$$\chi_{st} = \tilde{\chi}_{SGS} \times \frac{exp[-2(\mathrm{erf}^{-1}(1 - 2Z_{st}))^2]}{exp[-2(\mathrm{erf}^{-1}(1 - 2\tilde{Z}))^2]} \tag{4}$$

where $\tilde{\chi}_{SGS}$ is the LES-filtered subgrid-scale value of scalar dissipation rate. We also write: $\tilde{\chi}_{SGS} = 2((\nu/Pr) + (\nu_t/Pr_t))|\nabla\tilde{Z}|^2$, where ν is the molecular viscosity, Pr the Prandtl number, ν_t the turbulent viscosity and Pr_t a turbulent Prandtl number ($Pr_t = 1$).

Flame re-ignition is simply treated via a critical temperature criterion: $FIF = 0$ if $\tilde{T} \leqslant T_{ign}$ and $FIF = 1$ if $\tilde{T} \geqslant T_{ign}$, where $\tilde{T}$ is the (LES-filtered) temperature and T_{ign} its critical value at re-ignition; we use $T_{ign} = 1000$ K [22].

3. Results

FireFOAM was run using 16 processors on a large-scale Linux cluster; typical runs took on the order of 1000 h of CPU time.

While the present study is focused on evaluating simulations with thermally-driven MLR, a series of preliminary tests was also performed using a prescribed MLR approach in which $\dot{m}''_f$ is directly estimated from measured variations of the heptane pool mass [14,15]. Figure 3 presents the simulated time variations of the net total heat flux $\dot{q}''_s$ evaluated at the center of the fuel pan, as obtained in cases R1 and R2 and using a prescribed MLR approach; these variations are compared to measurements from a heat flux gauge. As mentioned in Section 2.3, the simulations suggest that the gas-to-liquid thermal load is dominated by radiative heat transfer and that convective heat

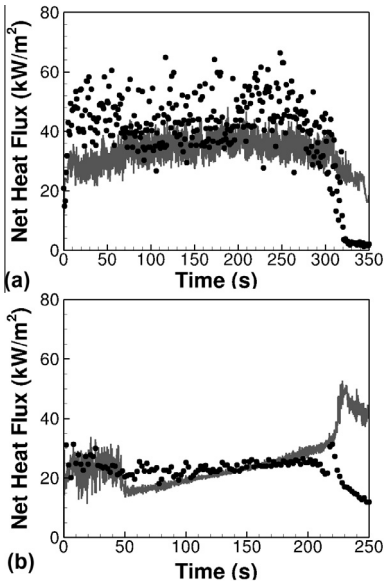

Fig. 3. Net heat flux at the center of the fuel pan. Comparison between experimental data (symbols) and numerical results (solid lines; prescribed MLR tests). Cases: (a) R1; (b) R2.

transfer has limited impact; in the present small-scale (optically-thin) compartment, radiative heat transfer is controlled by the flame emissive power and by the wall temperatures. Figure 3 shows that heat flux variations feature a fast initial transient followed by a fully-developed phase and by a decay phase. The agreement between experimental data and numerical results is good during the fully-developed phase: the order of magnitude of the heat flux is correctly predicted (typical values of $\dot{q}''_s$ range from 15 to 50 kW/m^2); discrepancies may be substantial for a particular case (for instance, in case R1, the simulated heat flux is under-estimated by approximately 30% on average) but the overall qualitative trends are correctly captured. Note, however, that the comparison between experimental data and numerical results is poor during the decay phase: in the (prescribed-MLR) simulations, residual flames are sustained until complete fuel depletion and $\dot{q}''_s$ remains large, whereas in the experiments, flames are extinguished once evaporation becomes sufficiently weak and $\dot{q}''_s$ becomes low. Overall, these preliminary tests are encouraging and demonstrate that FireFOAM is capable of simulating the intensity of the thermal feedback (at least during the fully-developed phase), which is a pre-requisite to using a thermally-driven MLR approach.

We now turn to a discussion of simulations with thermally-driven MLR. Note that to provide numerical start of evaporation, a prescribed-MLR model is applied during the first 5 s of the simulations. We first consider case R1 (Fig. 4). Case R1 is representative of over-ventilated fire conditions for which combustion is fuel-limited and the flame is stabilized above the fuel source. Figure 4(a) shows that fuel evaporation is well predicted: during the fully developed stage, the discrepancies between measured and simulated MLR are less than 30% (the discrepancies are larger during the decay phase). Figure 4(a) also shows that case R1 is extinction-free and that the spatially-averaged rate of production of non-burning fuel $(C_7H_{16})^*$ is 0, $\dot{\Omega}_{(C_7H_{16})*} = {}_V\overline{(\dot{\omega}'''_{GR2}} - \overline{(\dot{\omega}'''_{GR2}}\,dV = 0$ where V is the volume of the fire compartment. Figure 4(b) presents the corresponding variations of the simulated heat release rate, noted HRR, HRR $= {}_V\overline{(\dot{\omega}'''_{h_s}}\,dV$; these variations are compared to the fuel-limited estimate of HRR, noted HRR$_{FL}$ and defined as the product of MLR times the heat of combustion, HRR$_{FL}$ = MLR $\times\, \Delta H_F = (\dot{m}''_f \times A_f) \times \Delta H_F$. Figure 4(b) shows that in a time average sense HRR $\approx$ HRR$_{FL}$, which suggests that the combustion efficiency, noted χ_a and defined as the ratio of the time-integrated HRR divided by the time-integrated HRR$_{FL}$, is close to 1, $\chi_a = (\int_0^\infty HRR(t')dt' / \int_0^\infty HRR_{FL}(t')dt') \approx 1$.

Figure 4(c) presents the variations of temperature at selected representative locations. TC4 and TC9 are located near the vented wall, at 10 and

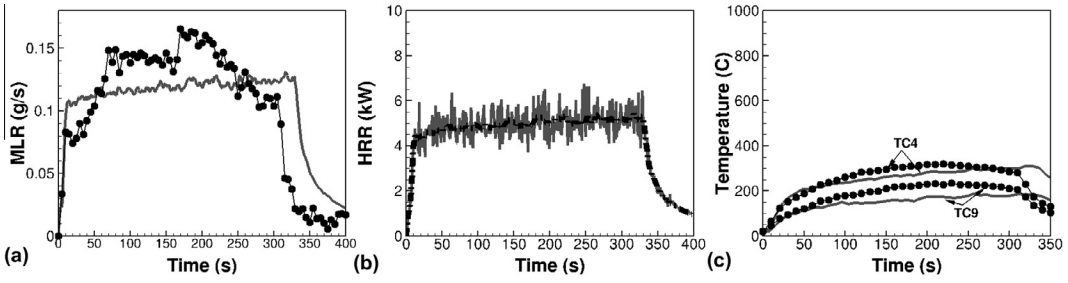

Fig. 4. Comparison between experimental data (symbols) and numerical results (solid lines) for case R1. (a) Measured and simulated MLR, also compared to the simulated rate of formation of non-burning fuel $\dot{\Omega}_{(C_7H_{16})*}$ (0 in case R1); (b) Simulated HRR (gray solid line) compared to its fuel-limited estimate HRR$_{FL}$ (black dashed line) (no experimental data in this plot); (c) Temperature (at TC4/TC9).

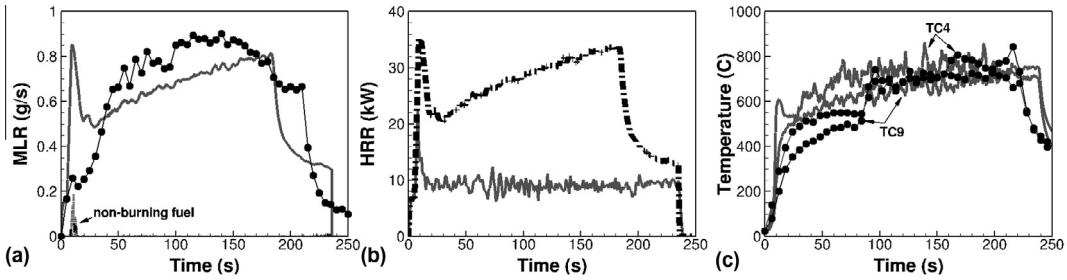

Fig. 5. Case R2, see caption of Fig. 4.

30 cm elevation respectively. Note that in Fig. 4(c), the experimental data correspond to raw thermocouple measurements and are not corrected for radiation losses; these raw data are compared to simulation results using a virtual thermocouple model [10]. Figure 4(c) shows that in case R1, because the fire is well-ventilated, the ceiling layer temperature remains moderate and is approximately equal to 300 °C; the oxygen mole fraction in the ceiling layer is close to 0.17. The agreement between experimental data and numerical results is very good.

Next we consider case R2 (Fig. 5). Case R2 is representative of under-ventilated fire conditions for which combustion becomes oxygen-limited and partial extinction is observed until the flame re-locates at the vents and continues burning extinction-free. Figure 5(a) shows that during the fully developed stage, fuel evaporation is again well predicted: discrepancies between measured and simulated MLR are less than 30%. Figure 5(a) also shows that case R2 features production of non-burning fuel (*i.e.*, flame extinction) during a short transient period at times $t \approx 10$–20 s; this transient period corresponds to the displacement of the flame from the heptane pool to the bottom and top vents.

Because HRR is defined as the heat release rate inside the fire compartment, and because except for a short transient period case R2 is extinction-free, the difference between HRR and HRR_{FL} (Fig. 5(b)) gives a measure of the relative weights of burning inside and outside of the fuel compartment; we find that 37% of the burning takes place inside. Note that, once the flame is successfully stabilized at the vents, it is supplied with fresh air and the combustion efficiency is close to 1; we find $\chi_a = 0.98$.

Figure 5(c) presents the variations of temperature at TC4/TC9 locations. In case R2, the compartment temperatures are high (approximately 700 °C) and the oxygen mole fractions are low (close to 0 in the ceiling layer). The agreement between experimental data and numerical results is good.

We now turn to case R4 (Fig. 6). Case R4 is representative of ultra-rich fire conditions for which the combustion is driven to a complete extinction due to oxygen starvation. Figure 6(a) shows that, while some details of the measured fluctuations in the fuel evaporation rate may not be simulated accurately, the simulation successfully captures the gradual reduction in MLR followed by a complete stop (at $t \approx 45$ s in FireFOAM *vs* at $t \approx 80$ s in the experiment). Figure 6(a) also shows that case R4 features production of non-burning fuel (*i.e.*, flame extinction) during a transient period at times $t \approx 20$–40 s; this transient period corresponds to a transition to complete flame extinction. Figure 6(b) supports these results and shows that HRR is 0 after $t = 40$ s. The discrepancy between HRR and HRR_{FL} in Fig. 6(b) gives a measure of the weight of flame extinction; we find $\chi_a \approx 0.87$. Figure 6(b)

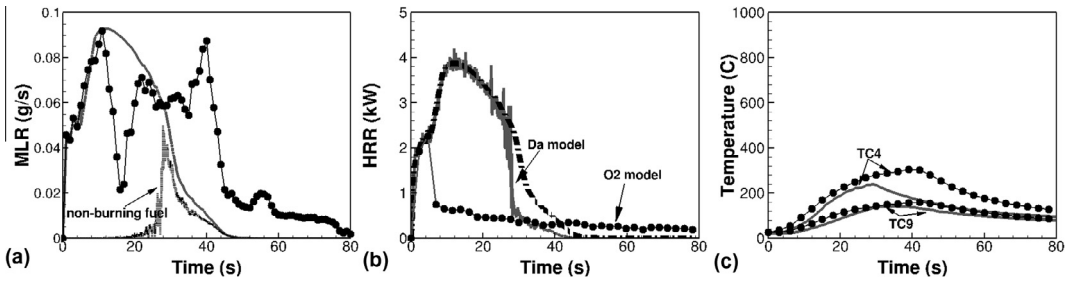

Fig. 6. Case R4, see caption of Fig. 4. The curve with dot symbols in Fig. (b) corresponds to results obtained from a test simulation using a simple oxygen-based flame extinction criterion.

also presents results obtained from a test simulation using a simple flame extinction criterion based on a critical value (15%) of the oxygen mole fraction. The test results are found to differ significantly from experimental data: extinction is overestimated (underestimated) at early (late) times; and in contrast to the experiment, full flame extinction is not observed.

Figure 6(c) presents the corresponding variations of temperature at TC4/TC9 locations. The agreement between experimental data and numerical results is fair.

4. Conclusion

The present study is aimed at evaluating the ability of current CFD-based fire models to simulate compartment fires under poorly ventilated conditions. The study considers four cases that are taken from a previously developed experimental database and are representative of four different flame behaviors, *i.e.*, steady over-ventilated fires, steady under-ventilated fires, unstable fires with partial flame quenching, transient fires leading to total flame quenching. The numerical simulations are performed with a CFD solver called FireFOAM and using a new flame extinction model as well as a thermally-driven fuel evaporation model. The flame extinction model is based on the concept of a critical value of the flame Damköhler number. Overall, the agreement between experimental and computational results is good and shows that current CFD-based fire models are capable of describing (at least qualitatively and to a certain extent, as documented in the paper, quantitatively) the transition from over- to under-ventilated fire conditions, as well as the transition from extinction-free conditions to conditions in which the flame experiences quenching. The numerical results also allow a discussion of combustion efficiency, a parameter that is of significant practical importance (for instance for problems related to smoke explosion or toxic emissions) but for which data are generally unavailable.

One open question that remains a concern is the level of grid resolution required for accurate simulations of gas-to-fuel-source heat fluxes (the thermal feedback). The present study is performed with a 1 cm grid resolution; this cell size is sufficient to capture flame scales but is not suitable to resolve vent flows or boundary layer flows. The relative success of the simulations may be due to a number of helpful factors. One factor is that the flames are characterized by small sizes (less than 10 kW) and are therefore unsteady laminar rather than fully turbulent; these flames do not feature a large range of length scales and do not represent a difficult computational challenge. Another factor is that radiation heat transfer apparently dominates the thermal feedback; in the present problem, radiation heat transfer is controlled by the flame and by the walls; and these features are suitably resolved by the computational grid.

Another open question is whether the new Damköhler-number-based flame extinction model performs better than previously established models based on the concept of a critical value of the flame temperature [13]. The present study does not answer that question (better resolved experimental data would be required) and this issue will be considered in future work.

Acknowledgements

This research project is funded by FM Global under the Strategic Research Program for Fire Modeling. This project is also part of a university-industry partnership sponsored by the National Science Foundation (NSF-GOALI grant program; Award #1236788); the NSF-GOALI project is a joint collaboration between the Department of Fire Protection Engineering at UMD, FM Global, and United Technologies Research Center.

References

[1] A. Trouvé, Y. Wang, *Intl. J. Comput. Fluid Dyn.* 24 (2010) 449–466.
[2] F.A. Williams, *Combustion Theory*, second ed., Addison Wesley, 1985.
[3] N. Peters, *Turbulent Combustion*, Cambridge University Press, 2000.
[4] C.K. Law, *Combustion Physics*, Cambridge University Press, 2006.
[5] B.H. Chao, C.K. Law, J.S. T'ien, *Proc. Combust. Inst.* 23 (1990) 523–531.
[6] J.S. T'ien, H. Bedir, Proc. 1st Asia-Pacific Conf. Combust., Osaka, Japan, 1997, pp. 345–352.
[7] J.L. Rhatigan, H. Bedir, J.S. T'ien, *Combust. Flame* 112 (1998) 231–241.
[8] P. Narayanan, H.R. Baum, A. Trouvé, *Proc. Combust. Inst.* 33 (2011) 2539–2546.
[9] V.R. Lecoustre, P. Narayanan, H.R. Baum, A. Trouvé, Fire Safety Science – Proc. Tenth Intl. Symposium, International Association for Fire Safety Science, 2011, pp. 583–595.
[10] N. Ren, Y. Wang, S. Vilfayeau, A. Trouvé, *Combust. Flame* (2014) submitted for publication.
[11] FM Global, *FireFOAM*, <http://code.google.com/p/firefoam-dev/>.
[12] Z. Hu, Y. Utiskul, J.G. Quintiere, A. Trouvé, Fire Safety Science – Proc. Eighth International Symposium, International Association for Fire Safety Science, 2005, pp. 1193–1204.
[13] Z. Hu, Y. Utiskul, J.G. Quintiere, A. Trouvé, *Proc. Combust. Inst.* 31 (2007) 2537–2545.
[14] Y. Utiskul, Extensive Study of Wall-Vent Compartment Fire Behavior Under Limited Ventilation, MS Thesis, University of Maryland at College Park, 2003.

[15] Y. Utiskul, J.G. Quintiere, A.S. Rangwala, B.A. Ringwelski, K. Wakatsuki, T. Naruse, *Fire Safety J.* 40 (2005) 367–390.
[16] Y. Wang, P. Chatterjee, J.L. de Ris, *Proc. Combust. Inst.* 33 (2011) 2473–2480.
[17] OpenCFD Ltd., *OpenFOAM*, <http://www.openfoam.com/>.
[18] C. Fureby, G. Tabor, H.G. Weller, A.D. Gosman, *Phys. Fluids* 9 (1997) 3578–3580.
[19] B.F. Magnussen, B.H. Hjertager, *Proc. Combust. Inst.* 16 (1976) 719–729.
[20] A. Hamins, M. Klassen, J. Gore, T. Kashiwagi, *Combust. Flame* 86 (1991) 223–228.
[21] R. Seiser, L. Truett, D. Trees, K. Seshadri, *Proc. Combust. Inst.* 27 (1998) 649–657.
[22] J.C. Hewson, A.R. Kerstein, *Combust. Sci. Technol.* 174 (2002) 35–66.